Available online at www.sciencedirect.com
SCIENCE DIRECT®
Fluid Dynamics Research 37 (2005) 357–373
FLUID DYNAMICS RESEARCH

Magnetohydrodynamic flow around a sphere

T.V.S. Sekhar[a,*], R. Sivakumar[b], T.V.R. Ravi Kumar[c]

[a] *Department of Mathematics, Pondicherry Engineering College, Pondicherry 605 014, India*
[b] *Department of Physics, Pondicherry Engineering College, Pondicherry 605 014, India*
[c] *Department of Applied Mathematics, Ideal College of Arts and Sciences, Kakinada 533 003, India*

Accepted 10 May 2005

Communicated by M.S. Chong

Abstract

The flow of an incompressible, viscous, electrically conducting fluid past a sphere in an aligned magnetic field is investigated using the finite difference method for Re 100 and 200 and interaction parameter N in the range $0 \leqslant N \leqslant 10$ (or $0 \leqslant M \leqslant 100$), where M is the Hartmann number defined by $M = \sqrt{2N\,Re}$. The length of the recirculation bubble in the flow reduces monotonically with increasing magnetic field up to $N = 1$ and starts growing when $N \geqslant 2$. A non-monotonic behavior of the boundary layer separation angle is found when $N < 1$, where the backward movement of the separation angle is observed. For higher values of N, a linear dependence with $\sqrt{N}$ of the pressure drag coefficient, the total drag coefficient and the rear pressure is found. With increasing values of N, a general increase in upstream base pressure and a decrease in downstream base pressure is noted. The features found in this work are in agreement with those of experimental findings.

Keywords: Incompressible flow; Aligned magnetic field; Sphere; Defect correction; Multigrid method

1. Introduction

In the problem of viscous flow around a sphere, as the Reynolds number is increased, the wake behind a sphere undergoes a series of well-defined transitions on its way to becoming fully turbulent. The attached separation bubble grows in length until the Reynolds number reaches approximately 210. The

* Corresponding author. Tel.: +413 2656312.
E-mail addresses: sekhartvs@yahoo.co.in (T.V.S. Sekhar), sivtex@mailcity.com (R. Sivakumar), tvrravikumar@yahoo.com (T.V.R. Ravi Kumar).

0169-5983/$30.00 © 2005 Published by The Japan Society of Fluid Mechanics and Elsevier B.V.

doi:10.1016/j.fluiddyn.2005.08.003

first transition involves a (regular) symmetry-breaking topological change from a steady axisymmetric wake with an attached separation bubble to a steady non-axisymmetric wake consisting of a shortened separation bubble with two trailing counter-rotating vortices. In experimental visualizations, the dye is trapped in the vortex cores and this leads to a dramatic two-threaded structure. Johnson and Patel (1999) numerically found that this transition occurs at approximately $Re = 211$. This value compares well with the value determined by Tomboulides et al. (1993) and Tomboulides and Orszag (2000) ($Re = 212$). These values are consistent with experimental predictions which tend to be lower, but have an upper limit closer to the numerical estimates. Magarvey and Bishop (1961a, b) found the two-threaded wake to exist in the range $210 < Re < 270$, Nakamura (1976) found the transition occurred at $Re = 190$, and Ormieres and Provansal (1999) observed the two threads between $180 < Re < 280$. In addition, the stability analysis of Natarajan and Acrivos (1993) revealed a regular, i.e., time-steady transition at $Re = 210$.

The second topological transition is from the steady two-threaded wake to a periodic wake in which the trailing vortices form kinks that develop into strongly skewed loops, and these move away downstream. There have been various studies documenting and analyzing this transition. The critical Reynolds number has been determined experimentally to be: 280 (Ormieres and Provansal, 1999); 300 (Sakamoto and Haniu, 1995); between 270 and 290 by Magarvey and Bishop (1961a, b) and in the range 200–300 in the older study by Taneda (1978). Numerical simulations predict values $Re = 270$ (Johnson and Patel, 1999), and in the range 250–280 (Tomboulides et al., 1993). In addition, the stability analysis of Natarajan and Acrivos (1993) found the transition to occur at $Re = 277$, although they based the stability analysis on an axisymmetric base flow. Sungsu Lee (2000) has reported that the flow past a sphere remains two-dimensional and axisymmetric until $Re = 250$, and also that the periodic vortex shedding does not appear until $Re = 375$. Recently, Thompson et al. (2001) studied the kinematics and dynamics of sphere wake transition.

1.1. Effect of magnetic field on the flow

An externally applied magnetic field can significantly control the nature of flow of an electrically conducting fluid. Experimentally, it is well established that two-dimensional instabilities can be suppressed by the application of the external magnetic field. In general, it is believed in magnetohydrodynamics (Chandrasekhar, 1981) that a steady magnetic field can damp any instability in the flow structure. The effect of a magnetic field on Stokes flow past a sphere in a conducting fluid is studied by Chester (1957) for low Reynolds numbers. The flow of an incompressible viscous electrically conducting fluid past a sphere, in the presence of a uniform magnetic field parallel to the undisturbed flow using Oseen approximation, has been investigated by Gotoh (1960) and later by Goldsworthy (1962). The force exerted on the sphere for various conductivities and Reynolds numbers is computed by Blerkom (1960). For the case of flow around a circular cylinder, Leibovich (1967) proved that the separation at a rear stagnation point could be suppressed by a sufficiently large magnetic field perpendicular to the surface of the cylinder. These are further discussed by Buckmaster (1969, 1971). From the works of Leibovich (1967) and Buckmaster (1969, 1971) it is clear that the boundary layer separation will not occur if the magnetic field is large enough. Banks and Zaturska (1984) examined the flow structure at a rear stagnation point of an incompressible viscous and electrically conducting fluid and provided a resolution of the differences between the works of Leibovich and that of Buckmaster.

Some recent investigations carried out with regard to the problem of flow around a circular cylinder with magnetic field are as follows: Mutschke et al. (1997, 1998, 2001) investigated the two- and three-dimensional instabilities of the cylinder wake in an aligned magnetic field, the cylinder wake control by magnetic fields in liquid metal flows and a linear stability analysis of the three-dimensional instabilities of the cylinder wake. Further, the control of flow separation using electromagnetic forces has been discussed by Weier et al. (2003). Sekhar et al. (2003) solved the vorticity–stream function form of the Navier–Stokes equations for the steady viscous incompressible magnetohydrodynamic flow past a sphere using the finite difference method (not second-order accurate) and found the suppression of the separation at rear stagnation point and increase of drag coefficient with the increase of the magnetic field for moderate values of Re and low values of N. Besides these theoretical studies, a few experimental investigations are also reported in the literature by Yonas (1967), Maxworthy (1968, 1969), Lahjomri (1984,1993) and Josserand et al. (1993) as follows.

Maxworthy achieved pressure distribution measurements around a sphere placed in a sodium flow aligned with the magnetic field at infinity with the interaction parameter ranging from 0 to 40. The main conclusions of Maxworthy (1968, 1969) are as follows: the upstream pressure first continuously rises as N increases and reaches an asymptotic value for N greater than approximately 15. The downstream base pressure decreases as N increases due to the loss in total pressure head that a fluid particle undergoes when crossing the magnetic field. The association of these two phenomena is consequently responsible for an increase with N of the pressure drag coefficient, which was found proportional to $\sqrt{N}$ as soon as N is greater than 5. A similar behavior has also been reported by Yonas (1967) who made direct drag measurements on spheres and disks in a sodium flow for interaction parameter values up to 80, where the drag coefficient was found to be $3.3\sqrt{N}$ ($N > 10$) for spheres. The fact that the asymptotic dependence with N of the drag coefficient seems to be independent of the body's shape is probably one of the most important results of this study. Lahjomri (1984) experimentally found that, for a fixed hydrodynamic Reynolds number, an increase of the interaction parameter above a critical value was able to suppress the vortex street in the wake.

The angular evolution of the pressure around a cylinder in a magnetohydrodynamic flow aligned with the magnetic field for $0 \leqslant N \leqslant 8$ has been studied experimentally by Josserand et al. (1993) who found that for $N < 1$, both the front and rear pressure increases when compared to the no field case $N = 0$. For $N > 1$, the upstream base pressure increases with N while the downstream base pressure decreases. Further, it is also shown that for sufficiently large fields, the von Kármán street behind the cylinder could be suppressed.

In the present paper, the incompressible conducting fluid flow past a sphere in the presence of an applied magnetic field parallel to the main flow is investigated for the Reynolds numbers 100 and 200 using the finite difference method solved by the multigrid method. The defect correction technique is then employed to achieve second-order accurate results. We verified our results first with no magnetic field case where results are available in the literature up to high Reynolds numbers $100 \leqslant Re \leqslant 5000$ by Fornberg (1988).

2. Problem definition

The flow of steady incompressible viscous conducting fluid past a sphere with uniform free-stream velocity U_∞ (from left to right) and an aligned uniform magnetic field H_∞ is considered for this study.

The equation of continuity is satisfied by introducing the dimensionless stream function $\psi(r, \theta)$ defined by the equations

$$u = \frac{1}{r^2 \sin\theta}\frac{\partial\psi}{\partial\theta}, \quad v = \frac{-1}{r \sin\theta}\frac{\partial\psi}{\partial r}, \tag{1}$$

where u and v are the dimensionless radial and transverse components of velocity obtained by dividing the corresponding dimensional components by the stream velocity U_∞. The viscosity, density and conductivity of the fluid are μ, ρ and σ, respectively. The curl of the momentum equation is

$$\nabla \times \boldsymbol{\omega} \times \boldsymbol{q} = \frac{2}{Re}\nabla^2\boldsymbol{\omega} + N\,\nabla \times \{(\boldsymbol{q} \times \boldsymbol{H}) \times \boldsymbol{H}\}, \tag{2}$$

where q is the fluid velocity, H is the magnetic field and

$$\boldsymbol{\omega} = \nabla \times \boldsymbol{q} \tag{3}$$

is the vorticity. The Reynolds number $Re = 2\rho U_\infty a/\mu$ (a is radius of the sphere) and the interaction parameter $N = \sigma H_\infty^2 a/\rho U_\infty$. The magnetic field and fluid flow are aligned at infinity and so the electric field can be assumed to be zero. The magnetic Reynolds number R_m (ratio of induced magnetic field to imposed magnetic field) is assumed to be small (< 1) so that the magnetic field is uniform and low enough for its effect to be treated as a small perturbation of the zero field potential flow. This enables us to replace the magnetic field in all MHD equations by

$$H = (-\cos\theta, \sin\theta, 0), \tag{4}$$

hence eliminating several non-linear terms of unknown quantities. Expanding (2) and (3) using (1) and (4) with spherical polar coordinates (r, θ, ϕ) (axis-symmetric), we get the Navier–Stokes equations in vorticity–stream function form as

$$\frac{\partial^2\psi}{\partial r^2} + \frac{1}{r^2}\frac{\partial^2\psi}{\partial\theta^2} - \frac{\cot\theta}{r^2}\frac{\partial\psi}{\partial\theta} = r\omega\sin\theta$$

and

$$\frac{\partial^2\omega}{\partial r^2} + \frac{2}{r}\frac{\partial\omega}{\partial r} + \frac{1}{r^2}\frac{\partial^2\omega}{\partial\theta^2} + \frac{\cot\theta}{r^2}\frac{\partial\omega}{\partial\theta} - \frac{\omega}{r^2\sin^2\theta} = \frac{Re}{2}\left(u\frac{\partial\omega}{\partial r} + \omega\frac{\partial u}{\partial r} + \frac{u\omega}{r} + \frac{v}{r}\frac{\partial\omega}{\partial\theta} + \frac{\omega}{r}\frac{\partial v}{\partial\theta}\right)$$
$$- \frac{NRe}{2r}\left(\frac{-r\sin 2\theta}{2}\frac{\partial u}{\partial r} + \frac{u}{2}\sin 2\theta - r\cos^2\theta\frac{\partial v}{\partial r}\right.$$
$$\left. - v\cos^2\theta + \sin^2\theta\frac{\partial u}{\partial\theta} + v\cos 2\theta + \frac{\sin 2\theta}{2}\frac{\partial v}{\partial\theta}\right).$$

Because the stream function and vorticity are expected to vary most rapidly near the surface of the sphere, we substitute $r = e^{\xi}$. Now, the above two equations become

$$\frac{\partial^2\psi}{\partial\xi^2} - \frac{\partial\psi}{\partial\xi} + \sin\theta\frac{\partial}{\partial\theta}\left(\frac{1}{\sin\theta}\frac{\partial\psi}{\partial\theta}\right) + \sin\theta e^{3\xi}\omega = 0, \tag{5}$$

$$\begin{aligned}&\frac{\partial^2\omega}{\partial\xi^2} + \frac{\partial\omega}{\partial\xi} + \cot\theta\frac{\partial\omega}{\partial\theta} + \frac{\partial^2\omega}{\partial\theta^2} - \frac{\omega}{\sin^2\theta}\\ &\quad = \frac{Re}{2}e^{\xi}\left(u\frac{\partial\omega}{\partial\xi} + v\frac{\partial\omega}{\partial\theta} - u\omega - v\omega\cot\theta\right)\\ &\qquad - \frac{N\,Re}{2}e^{\xi}\left[\frac{\sin 2\theta}{2}\left(-\frac{\partial u}{\partial\xi} + \frac{\partial v}{\partial\theta} + u\right) + \sin^2\theta\left(\frac{\partial u}{\partial\theta} - v\right) - \cos^2\theta\frac{\partial v}{\partial\xi}\right],\end{aligned} \tag{6}$$

where ψ and ω are dimensionless stream function and vorticity, respectively, and

$$u = \frac{e^{-2\xi}}{\sin\theta}\frac{\partial\psi}{\partial\theta}, \quad v = -\frac{e^{-2\xi}}{\sin\theta}\frac{\partial\psi}{\partial\xi}.$$

The boundary conditions to be satisfied are

$$\text{On the surface of the sphere } (\xi = 0): \quad \psi = \frac{\partial\psi}{\partial\xi} = 0, \quad \omega = -\frac{1}{\sin\theta}\frac{\partial^2\psi}{\partial\xi^2}.$$

$$\text{At large distances from the sphere } (\xi \to \infty): \quad \psi \sim \frac{1}{2}e^{2\xi}\sin^2\theta, \quad \omega \to 0.$$

$$\text{Along the axis of symmetry } (\theta = 0 \text{ and } \theta = \pi): \quad \psi = 0, \quad \omega = 0.$$

3. Numerical method

The governing partial differential equations (5) and (6) are solved by first applying finite difference method and the resulting algebraic equations are solved by using the multigrid method. The finite difference grid is shown in Fig. 1, where the flow is from left to right. All derivatives in the governing equations are approximated by second-order central differences except for the convective terms which are approximated by first-order upwind differences. This procedure is used to ensure diagonal dominance of the resulting algebraic system.

Here, a recursive multigrid procedure (V-cycle) is employed in which the smoother is a point Gauss Seidel iteration and the usual coarse grid correction (Juncu and Mihail, 1990) is applied. We used the injection operator as restriction operator throughout this study. The 9-point prolongation operator defined by Wesseling (1991) is used for the present study. The solution obtained by the multigrid method is not second-order accurate as we have approximated all terms by second-order central differences except convective terms which are approximated by first-order upwind difference scheme

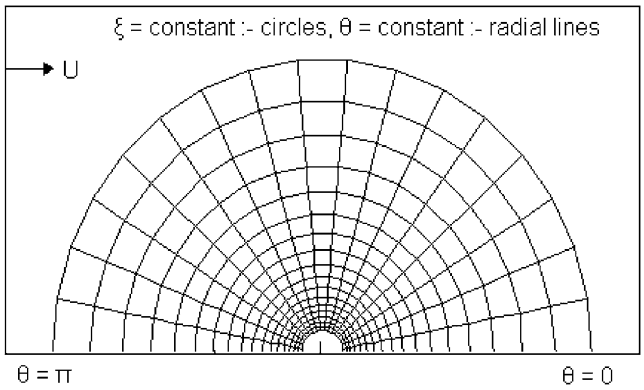

Fig. 1. Figure showing the type of grid used.

to ensure diagonal dominance. In order to achieve second-order accurate solution, the defect correction method is employed as follows. If **B** is the operator obtained, for example, by first-order upwind discretization and **A** is that obtained by second-order accurate discretization, then the defect correction algorithm works as given below. At the start of the defect correction, $\bar{y}$ is a solution that is not second-order accurate, and at the end of the defect correction, $\bar{y}$ is second-order accurate. In the algorithm given below, usually in practice, it is sufficient to take $n = 1$ or 2. In this study, we considered $n = 5$.

begin Solve $\mathbf{B}\bar{y} = b$
  for $i := 1$ **step** 1 **until** n **do**
    solve $By = b - A\bar{y} + B\bar{y}$
    $\bar{y} := y$
  od
end

The initial solution is taken as $\psi = 0$ and $\omega = 0$ at all inner grid points except for ψ at $\xi = \infty$, where the boundary condition holds. In finding the solution for higher values of *Re* and *N*, the solution obtained for lower values of *Re* and *N* are used as starting solution. Convergence is said to have been achieved when the norm of the dynamic residuals is less than 10^{-4} for $N \leqslant 1$. For $N > 1$, convergence criterion is chosen such that when the difference between two successive iterations at all interior grid points (for ψ and ω) is less than 10^{-7}.

4. Results and discussion

Results obtained from the finest grid 512×512 of the above multigrid procedure for the Reynolds numbers 100 and 200 and the interaction parameter $0 \leqslant N \leqslant 10$ are given. The interaction parameter N can be equivalently written in terms of Hartmann number M by the relation $M = \sqrt{2N\,Re}$. Theviscous

drag coefficient C_v, pressure drag coefficient C_p and surface pressure $P_{\xi=0}(\theta)$ are evaluated using the following relations:

$$C_v = -\frac{4}{Re}\int_0^{\pi} \omega_{\xi=0} \sin^2\theta \, d\theta,$$

$$C_p = \frac{2}{Re}\int_0^{\pi} \left\{ \left(\omega + \frac{\partial\omega}{\partial\xi}\right)_{\xi=0} \sin^2\theta \right\} d\theta,$$

$$P_{\xi=0}(\theta) = 1 + \frac{8}{Re}\int_0^{\infty} \left(\frac{\partial\omega}{\partial\theta}\right)_{\theta=\pi} d\xi + \frac{4}{Re}\int_{\pi}^{\theta} \left(\frac{\partial\omega}{\partial\xi} + \omega\right)_{\xi=0} d\theta.$$

First, we verified the problem for the case of zero magnetic field ($N = 0$) which corresponds to the steady incompressible viscous flow past a sphere and the results obtained on the separation length (l), separation angle (θ_s) and drag coefficients agree with the data available in the literature by Fornberg (1988). The comparison of the drag coefficients are given in Table 1. We then studied the flow patterns due to the magnetic field by increasing the value of N. For $N < 5$, the recirculation length, separation angle and drag coefficient values in two different grids 256×256 and 512×512 are tabulated in Tables 2 and 3. For $N \geqslant 5$, results are obtained from the finest grid of 512×512.

The streamlines for $Re = 100$ and 200 are presented in Figs. 2 and 3, respectively. The length of the recirculation bubble at rear stagnation point of the sphere reduces monotonically from $N = 0.01$ to 1. A similar phenomena is reported through numerical simulation by Raghava Rao and Sekhar (1995) in the problem

Table 1
Verification of the present results with the literature for the case of zero magnetic field

Re	Present results	Fornberg (1988)	Juncu and Mihail (1990)
100	0.52	0.54	0.53
200	0.36	0.37	–

Table 2
Comparison of second-order accurate separation length, separation angle and drag coefficient values in two different grids for $Re = 100$

N	l		θ_s		C_D	
	256×256	512×512	256×256	512×512	256×256	512×512
0.5	2.13	2.12	43.59	44.30	0.59	0.61
1	1.94	1.94	38.67	39.37	0.67	0.70
2	1.98	1.99	36.56	37.27	0.80	0.83
3	2.08	2.12	36.56	37.62	0.90	0.93
4	2.16	2.22	37.27	38.32	1.01	1.02

Table 3
Comparison of second-order accurate separation length, separation angle and drag coefficient values in two different grids for $Re = 200$

N	l		θ_s		C_D	
	256×256	512×512	256×256	512×512	256×256	512×512
0.5	3.17	3.07	54.84	55.19	0.43	0.45
1	2.87	2.84	49.92	50.27	0.51	0.53
2	2.91	2.94	46.41	47.11	0.62	0.65
3	3.04	3.10	46.41	47.11	0.71	0.74
4	3.11	3.23	46.41	47.46	0.78	0.82

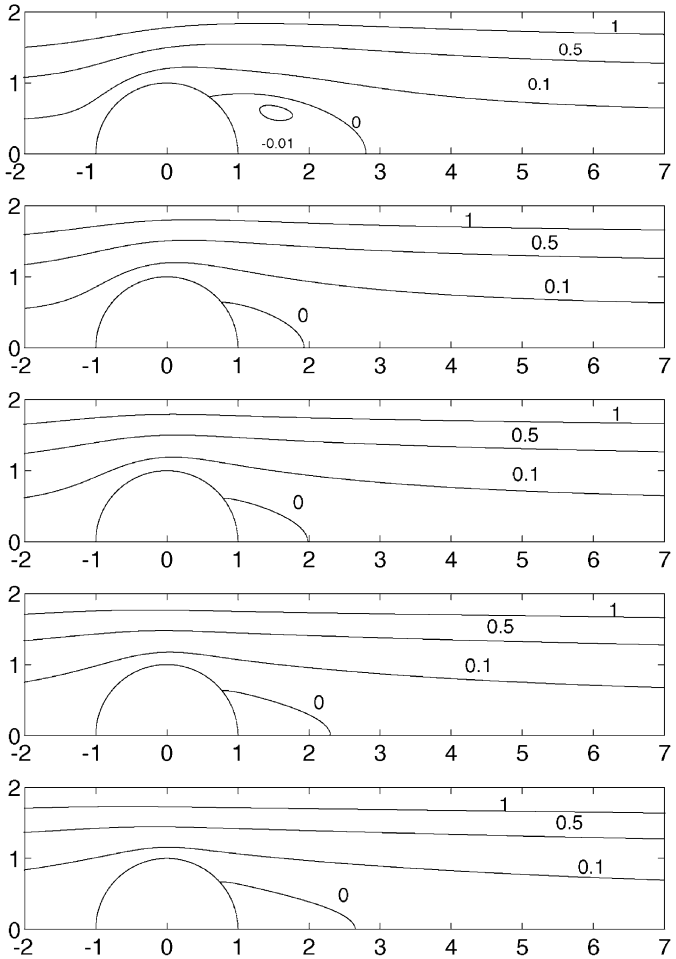

Fig. 2. Streamlines of the flow with $Re = 100$ with $N = 0, 1, 2, 5, 10$.

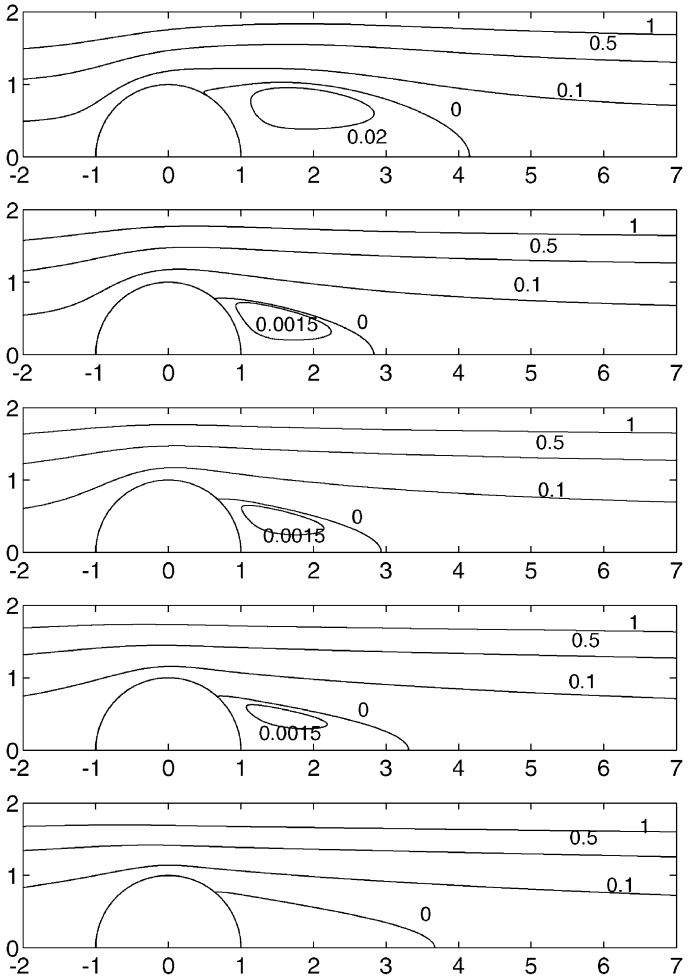

Fig. 3. Streamlines of the flow with $Re = 200$ with $N = 0, 1, 2, 5, 10$.

of translation of a sphere in a rotating viscous fluid, where inverse Rossby number affects the wake length. However, for stronger magnetic fields the separation is not finally suppressed. For magnetic fields strength given by $N > 1$, the wake length increases until $N = 10$. It is found that the boundary layer separation angle continuously decreases from $N = 0.01$ to 2 and then increases with increasing magnetic field for $Re = 100$. But for $Re = 200$, a non-monotonic behavior is observed in the boundary layer separation angle when $N < 1$. Although the separation angle generally decreases with N up to 2, an increase of the boundary layer separation angle is observed at $N = 0.4$. It is found that the boundary layer separation angle has moved 4° backward ($\theta = 0$ is the downstream region). A similar observation is reported through experimental studies by Maxworthy (1968). Further, Josserand et al. (1993) has verified the recession of boundary layer separation angle by 15° backward in the study of pressure and drag measurements on a cylinder in a liquid metal flow in the presence of an external magnetic field. Beyond $N > 2$, the boundary

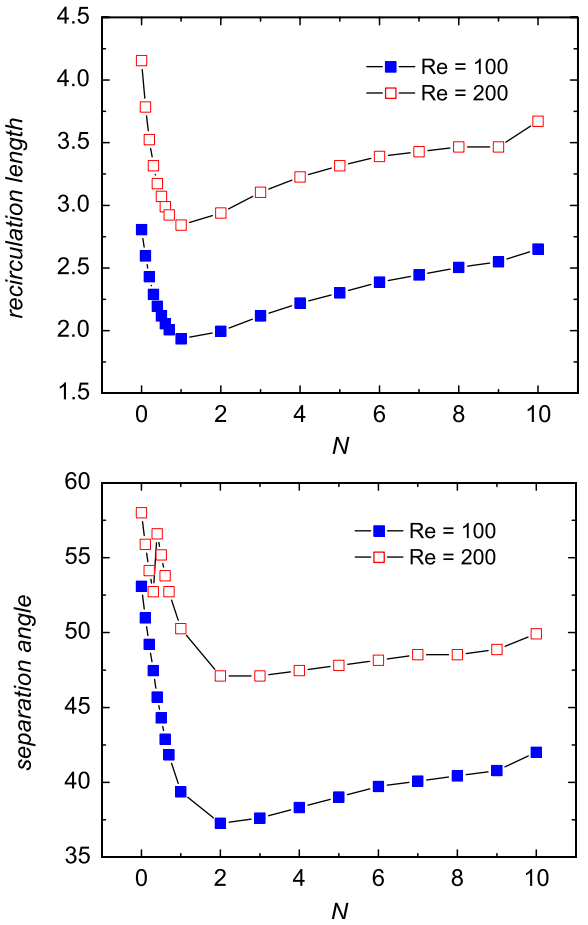

Fig. 4. Recirculation length versus N (top) and separation angle versus N (bottom).

layer separation angle increases and the flow becomes straightened in the main-stream direction and the curvature of the recirculation bubble (i.e., $\psi = 0$) decreases. The flow inside the recirculation bubble slows down monotonically with increasing magnetic field. The non-monotonic behavior in separation length and separation angle was also recently found by Mutschke et al. (2001) for the case of flow around a circular cylinder at $Re = 200$. Fig. 4 gives the overall picture on the behavior of wake length l and separation angle θ_s for different Reynolds numbers.

Fig. 5 shows the variation of pressure over the surface of the sphere. As can be seen from this figure, a general base pressure increase is found on both the upstream and downstream faces of the sphere for $Re = 100$ at very low values of N (< 0.1) (see inset in Fig. 5). For $N > 0.1$, the upstream base pressure increases and downstream base pressure decreases continuously for both $Re = 100$ and 200. The surface pressure at $\theta = 90°$ is found to first increase with N until $N \approx 3$ and then decrease with further increase of N. In fact, the suction force experienced by the rear half of the obstacle (here, sphere) first begins to slightly decrease when N increases and then increases continuously. A similar remark is reported by

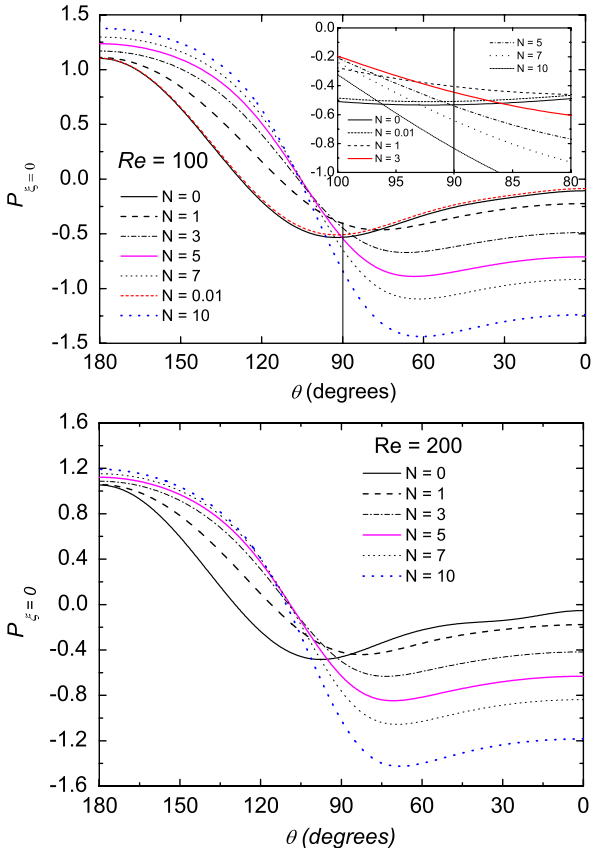

Fig. 5. Surface pressure for $Re = 100$ and 200.

Maxworthy (1968) from a study of the pressure distribution over the front half of the hemisphere–cylinder combination in an aligned field, where the author concludes that at $\theta = 90°$, the non-dimensional pressure coefficient was observed to first increase and then decrease with N. The same remark is also reported by Yonas (1967) and Lahjomri (1984).

4.1. Vortices and drag coefficient

Since the magnetic forces are proportional to and resist the flow of fluid in any other direction than that of the unperturbed magnetic field, near the sphere, they produce a change in the pattern of the lines. The length of the standing vortex reduced slightly and the strength of the disturbance in front and rear of the sphere is increased with increasing magnetic field (Figs. 7). The surface vorticity ($\omega_{\xi=0}$) for $Re = 100$ and 200 are presented in Fig. 6. From Figs. 6 and 7, it is clear that the magnetic field tends to suppress the fluctuations in surface vorticity behind the sphere. The pressure and viscous components of the drag coefficient and total drag coefficient as a function of N are presented in Fig. 8. The drag coefficient is found to increase continuously with N for all Re considered in this study. The variation of total drag

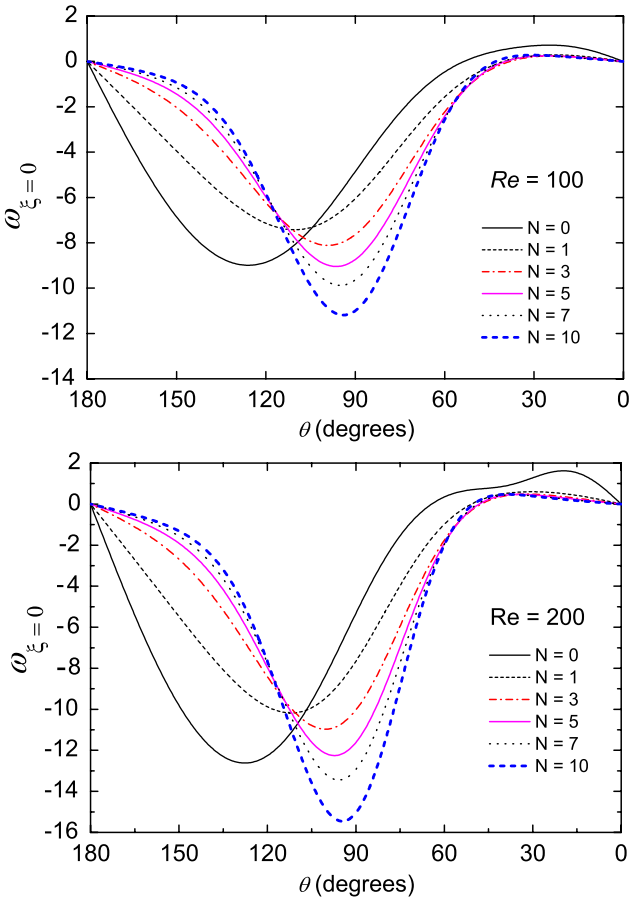

Fig. 6. Surface vorticity for $Re = 100$ and 200.

coefficient with Reynolds number is depicted in Fig. 9, where it is observed that for a given value of N, the drag coefficient decreases with increasing Re. The pressure drag coefficient C_p, the total drag coefficient C_D and the pressure at rear stagnation point $p(0, 0)$ are found to vary with $\sqrt{N}$ for $N \geqslant 5$. This behavior can be seen in Figs. 9 and 10. The results of the linear fit between C_D and $\sqrt{N}$ is tabulated in Table 4. In this table, B represents the proportionality constant, and it is nearly a constant equal to 0.36, independent of the Reynolds number. Yonas (1967), in his experiments on direct drag measurements on spheres and disks in a sodium flow, found that $C_D = 0.33\sqrt{N}$. The constant decrease of the base pressure for high N is the major source of the increase in the overall drag coefficient C_D. For these values of N, the losses in total pressure suffered along the front streamlines under the effect of the $\mathbf{j} \times \mathbf{B}$ forces, are responsible for the rear pressure drop. This behavior is responsible for the increase of pressure drag coefficient which in turn increases total drag coefficient. It is also found that the pressure at the rear stagnation point falls according to the $\frac{1}{2}$-power law with N, that is $p(0, 0) \propto \sqrt{N}$. Such a behavior is also reported experimentally by Josserand et al. (1993). From the plots of angular evolution of surface pressure, it is observed that compared to the case of no magnetic field, the increase of front pressure

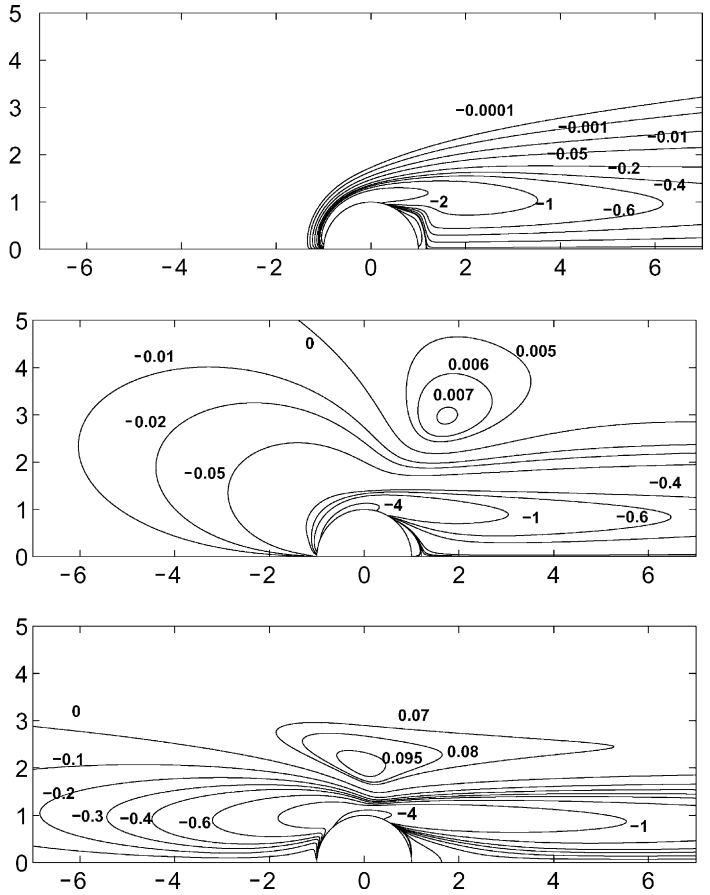

Fig. 7. Isocontours of vorticity of the flow with $Re = 200$ with $N = 0$, 1, 10.

around the front stagnation point is in agreement with the hypothesis of Maxworthy (1968, 1969) and Josserand et al. (1993) that a stagnant flow develops upstream of the sphere when the magnetic field is increased.

5. Conclusion

The steady, incompressible, axisymmetric conducting fluid flow around a sphere with an external magnetic field parallel to the main flow is investigated for the Reynolds numbers 100 and 200 and interaction parameter (N) up to 10 using the finite difference method. When $N < 1$, the backward movement of the separation angle is found for $Re = 200$. For $Re = 100$ and 200 a non-monotonic behavior in separation length is found. The separation length at rear stagnation point suppresses up to $N = 1$, beyond which it increases. The pressure drag coefficient, total drag coefficient and the pressure at rear stagnation point varies with $\sqrt{N}$.

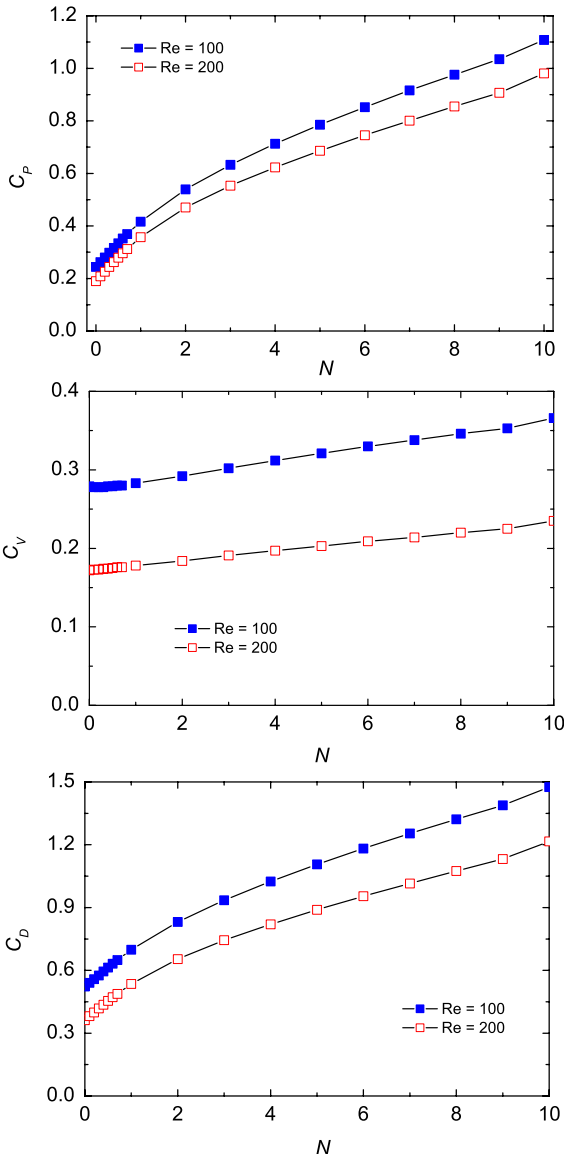

Fig. 8. (Top) Pressure and (middle) viscous components of drag coefficient as a function of interaction parameter; (bottom) drag coefficient versus interaction parameter.

Acknowledgements

The authors are thankful to Prof. Umamaheswara Rao, Department of Applied Mathematics, Andhra University, Visakhapatnam and Prof. G. Vaidyanathan, Department of Physics, Pondicherry Engineering College, Pondicherry, for useful discussion and encouragement. The authors are also grateful to Prof. A.S. Gupta, Professor Emeritus, I.I.T, Kharagpur for suggesting this problem.

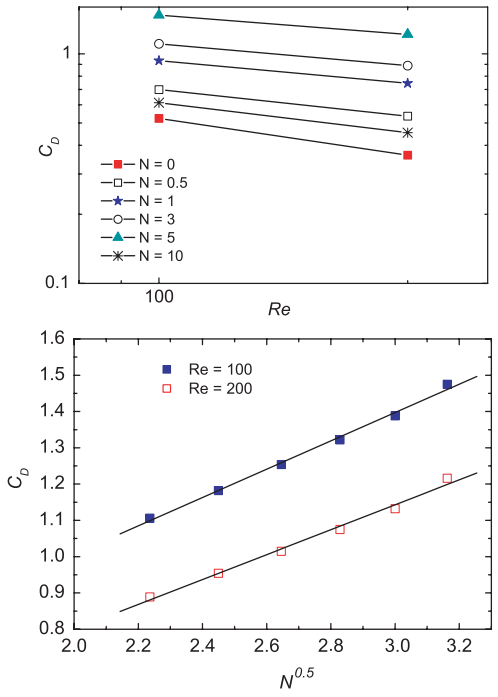

Fig. 9. (Top) Drag coefficient as a function of Reynolds number; (bottom) drag coefficient versus $\sqrt{N}$.

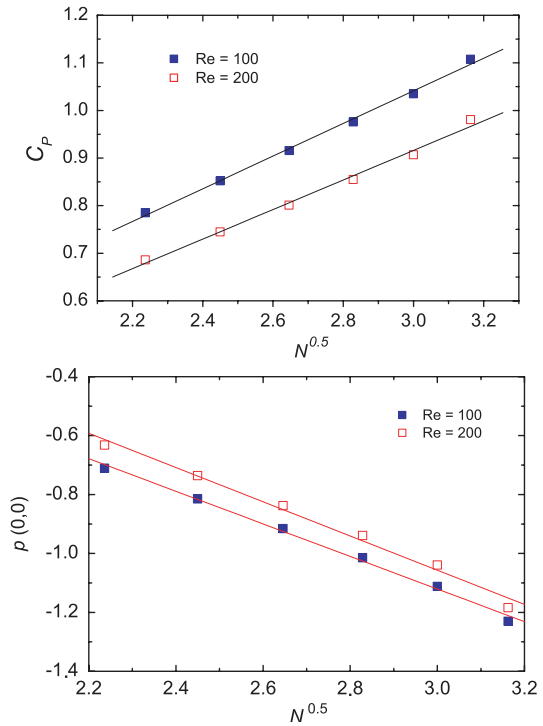

Fig. 10. Linear dependence of (top) pressure drag C_p; (bottom) pressure at rear stagnation point $p(0, 0)$ with $\sqrt{N}$.

Table 4
Results of fitting drag coefficient data C_D to the linear relation $C_D = A + B\sqrt{N}$

Reynolds number	A	B	Correlation coefficient
100	0.2260	0.390	0.998
200	0.1127	0.343	0.996

References

Banks, W.H.H., Zaturska, M.B., 1984. The flow of a electrically conducting fluid at a rear stagnation point. Z. Angew Math. Phys. 35, 72–80.

Blerkom, R.V., 1960. Magnetohydrodynamic flow of a viscous fluid past a sphere. J. Fluid Mech. 8, 432–441.

Buckmaster, J., 1969. Separation and magnetohydrodynamics. J. Fluid Mech. 38, 481–498.

Buckmaster, J., 1971. Boundary layer structure at a magnetohydrodynamic near stagnation point. Q. J. Mech. Appl. Math. 24, 373–386.

Chandrasekhar, S., 1981. Hydrodynamic and Hydromagnetic Stability. Dover, New York.

Chester, W., 1957. The effect of a magnetic field on Stokes flow on a conducting fluid. J. Fluid Mech. 3, 304.

Fornberg, B., 1988. Steady viscous flow past a sphere at high Reynolds numbers. J. Fluid Mech. 190, 471–489.

Goldsworthy, 1962. Magnetohydrodynamic flows of a perfectly conducting viscous fluid. J. Fluid Mech. 11, 519.

Gotoh, K., 1960. Magnetohydrodynamic flow past a sphere. J. Phys. Soc. Jpn. 15, 189–196.

Johnson, T.A., Patel, V.C., 1999. Flow past a sphere up to a Reynolds number of 300. J. Fluid Mech. 378, 19–70.

Josserand, J., Marty, Ph., Alemany, A., 1993. Pressure and drag measurements on a cylinder in a liquid metal flow with an aligned magnetic field. Fluid Dyn. Res. 11, 107–117.

Juncu, G.H., Mihail, R., 1990. Numerical solution of the steady incompressible Navier Stokes equations for the flow past a sphere by a multigrid defect correction technique. Int. J. Numer. Methods Fluids 11, 379–395.

Lahjomri, J., 1984. Caractèrisation de la structure des sillages amont et aval d'un cylindre á petit nombre de Renolds magnétique. Ph.D. Thesis, Grenoble University.

Lahjomri, J., Caperan, P., Alemany, A., 1993. The cylinder wake in a magnetic field aligned with velocity. J. Fluid Mech. 253, 421.

Leibovich, S., 1967. Magnetohydrodynamic flow at a rear stagnation point. J. Fluid Mech. 29, 401–413.

Magarvey, R.H., Bishop, R.L., 1961a. Transition ranges for three-dimensional wakes. Canadian J. Physics 39, 1418–1422.

Magarvey, R.H., Bishop, R.L., 1961b. Wakes in liquid-liquid systems. Phys. Fluids 4, 800–805.

Maxworthy, T., 1968. Experimental studies in magneto-fluid dynamics: pressure distribution measurements around a sphere. J. Fluid Mech. 31, 801–814.

Maxworthy, T., 1969. Experimental studies in magneto-fluid dynamics: flow over a sphere with a cylindrical afterbody. J. Fluid Mech. 35, 411–416.

Mutschke, G., Gerbeth, G., Shatrov, V., Tomboulides, A., 1997. Two- and three-dimensional instabilities of the cylinder wake in an aligned magnetic field. Phys. Fluids 9, 3114–3116.

Mutschke, G., Shatrov, V., Gerbeth, G., 1998. Cylinder wake control by magnetic fields in liquid metal flows. Exp. Therm. Fluid Sci. 16, 92–99.

Mutschke, G., Gerbeth, G., Shatrov, V., Tomboulides, A., 2001. The scenario of three-dimensional instabilities of the cylinder wake in an external magnetic field: a linear stability analysis. Phys. Fluids 13, 723–734.

Nakamura, I., 1976. Steady wake behind a sphere. Phys. Fluids 19, 1–18.

Natarajan, R., Acrivos, A., 1993. The instability of the steady flow past spheres and disks. J. Fluid Mech. 254, 323–344.

Ormieres, D., Provansal, M., 1999. Transition to turbulence in the wake of a sphere. Phys. Rev. Lett. 83, 80–83.

Raghava Rao, C.V., Sekhar, T.V.S., 1995. Translation of a sphere in a rotating viscous fluid: a numerical study. Int. J. Numer. Meth. Fluids 20, 1253–1262.

Sakamoto, H., Haniu, H., 1995. The formation mechanism and shedding frequency of vortices from a sphere in a uniform shear flow. J. Fluid. Mech. 287, 151–171.

Sekhar, T.V.S., Ravikumar, T.V.R., Kumar, H., 2003. MHD flow past a sphere at low and moderate Reynolds numbers. Comput. Mech. 31, 437–444.

Sungsu Lee, 2000. A numerical study of the unsteady wake behind a sphere in a uniform flow at moderate Reynolds numbers. Comput. Fluids 29, 639–667.

Taneda, S., 1978. Visual observations of the flow past a sphere at Reynolds numbers between 10^4 and 10^6. J. Fluid. Mech. 85, 187–192.

Thompson, M.C., Leweke, T., Provansal, M., 2001. Kinematics and dynamics of sphere wake transition. J. Fluids Struc. 15, 575–585.

Tomboulides, A.G., Orszag, S.A., 2000. Numerical investigation of transitional and weak turbulent flow past a sphere. J. Fluid Mech. 416, 45–73.

Tomboulides, A.G., Orszag, S.A., Karniadakis, G.E., 1993. Direct and large eddy simulations of axisymmetric wakes. AIAA Paper 93-0546.

Weier, T., Gerbeth, G., Mutschke, G., Lielausis, O., Lammers, G., 2003. Control of flow separation using electromagnetic forces. Flow Turbulence Combust. 71, 5–17.

Wesseling, P., 1991. Multigrid methods in fluid dynamics. In: Hackbusch, W., Trottenberg, U. (Eds.), Multigrid Methods-III. Springer, Berlin, p. T337.

Yonas, G., 1967. Measurements of drag in a conducting fluid with an aligned magnetic field and large interaction parameter. J. Fluid Mech. 30, 813–821.